Molecular Therapy
Nucleic Acids
Original Article

Exosomal miR-365a-5p derived from HUC-MSCs regulates osteogenesis in GIONFH through the Hippo signaling pathway

Ming-jie Kuang,[1,4] Kai-hui Zhang,[3,4] Jie Qiu,[1] An-bang Wang,[1] Wen-wen Che,[1] Xiao-ming Li,[2] Dong-li Shi,[1] and Da-Chuan Wang[1]

[1]Department of Orthopedics, The Provincial Hospital Affiliated to Shandong University, Shandong 250014, China; [2]Department of Orthopedics, Traditional Chinese Medicine-Western Medicine Hospital of Cangzhou City, Hebei Province 061000, China; [3]Department of Orthopedics, Tianjin Hospital, Tianjin 300211, China

The pathogenesis of glucocorticoid (GC)-induced osteonecrosis of the femoral head (GIONFH) is still disputed, and abnormal bone metabolism caused by GCs may be an important factor. *In vitro*, Cell Counting Kit-8 (CCK-8) and 5-ethynyl-2′-deoxyuridine (EdU) staining were used to evaluate cellular proliferation, and western blotting was used to investigate osteogenesis. *In vivo*, we used micro-computed tomography (micro-CT), H&E staining, Masson staining, and immunohistochemistry (IHC) analysis to evaluate the impact of exosomes. In addition, the mechanism by which exosomes regulate osteogenesis through the miR-365a-5p/Hippo signaling pathway was investigated using RNA sequencing (RNA-seq), luciferase reporter assays, fluorescence *in situ* hybridization (FISH), and western blotting. The results of western blotting verified that the relevant genes in osteogenesis, including BMP2, Sp7, and Runx2, were upregulated. RNA-seq and qPCR of the exosome and Dex-treated exosome groups showed that miR-365a-5p was upregulated in the exosome group. Furthermore, we verified that miR-365a-5p promoted osteogenesis by targeting SAV1. Additional *in vivo* experiments revealed that exosomes prevented GIONFH in a rat model, as shown by micro-CT scanning and histological and IHC analysis. We concluded that exosomal miR-365a-5p was effective in promoting osteogenesis and preventing the development of GIONFH via activation of the Hippo signaling pathway in rats.

INTRODUCTION

Osteonecrosis of the femoral head (ONFH) is caused by different factors impairing blood circulation to the femoral head, resulting in the ischemic necrosis of osteocytes and bone marrow components. Under the continuous stress of activity, the femoral head collapses, resulting in hip dysfunction. Glucocorticoids (GCs), a drug commonly used to treat rheumatoid diseases, are the main cause of GC-induced ONFH (GIONFH) following long-term use or the administration of large doses of GCs.[1] The symptoms of GIONFH in its early stages are not obvious, and methods for the diagnosis and treatment of GIONFH are limited. Once the femoral head collapses, it can only be treated with joint replacement, which imposes a huge economic burden on patients. Long-term extensive GC use can damage the local microcirculation of the femoral head, induce endoplasmic reticulum stress in osteoblasts and promote apoptosis, and result in an imbalance between adipogenesis and osteogenic differentiation in bone marrow mesenchymal stem cells (BMSCs). At present, it is thought that bone metabolism is closely related to the pathogenesis of GIONFH.[2] GC interference with normal bone metabolism may be the main cause of GIONFH.[3]

Exosomes are microvesicles with a diameter of less than 150 nm that contain nucleic acids, proteins, and lipids and are secreted by cells. They can regulate the local microenvironment, reduce inflammation, and promote tissue injury repair.[4,5] The relatively stable lipid bilayer structure of exosomes can effectively maintain the activity of their loaded contents, such as microRNA (miRNA or miR) and protein. As a result, exosomes are excellent intercellular materials transporters, and the RNA carried by exosomes has an angiogenesis-promoting effect.[6] However, few studies have focused on its therapeutic effects in GIONFH. Tao et al.[7] found that synovial MSC exosomes (MSC-Exos) are rich in Wnt5a and Wnt5b proteins, which can promote the proliferation and migration of chondrocytes by regulating the Wnt5a/YAP signaling pathway. In addition, exosomes derived from BMSCs carrying miR-122-5p promote the proliferation of osteoblasts in rabbits with ONFH via the RTK/Ras/mitogen-activated protein kinase (MAPK) signaling pathway.[8] These studies all

Received 11 February 2020; accepted 2 December 2020;
https://doi.org/10.1016/j.omtn.2020.12.006.

[4]These authors contributed equally

Correspondence: Da-Chuan Wang, Department of Orthopedics, The Provincial Hospital Affiliated to Shandong First Medical University, Jinan, Shandong 250014, China.
E-mail: wangdachuansd@163.com
Correspondence: Xiaoming Li, Department of Orthopedics, Traditional Chinese Medicine-Western Medicine Hospital of Cangzhou City, Hebei 061000, China.
E-mail: lixiaomingcz@126.com
Correspondence: Dong-li Shi, Department of Orthopedics, The Provincial Hospital Affiliated to Shandong First Medical University, Jinan, Shandong 250014, China.
E-mail: 192554798@qq.com

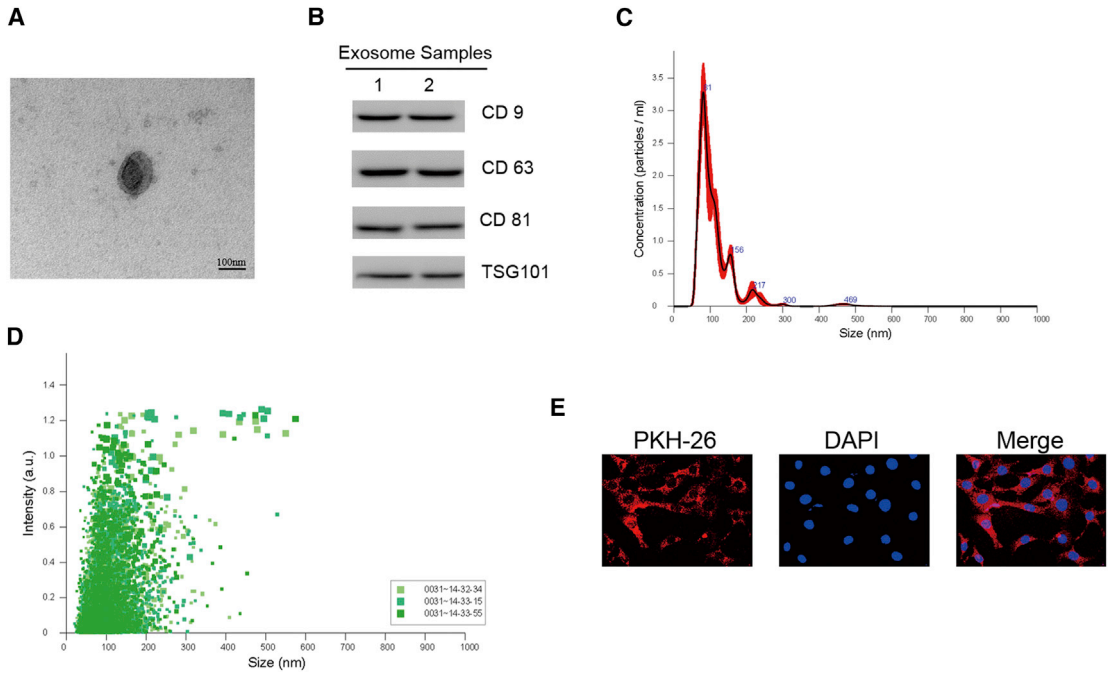

Figure 1. Exosomes extracted from HUC-MSCs were characterized using TEM, NanoSight analysis, and western blotting

(A) Morphology of HUC-MSC-Exos identified by transmission electron microscopy (TEM). Scale bar, 100 nm. (B) Western blot analysis of the surface biomarkers CD9, CD63, CD81, and TSG101. (C) Particle size distribution and concentration of HUC-MSC-Exos measured by NanoSight analysis. (D) The enrichment of exosomes was calculated using NanoSight analysis. (E) HUC-MSC-Exos were labeled with PKH26, and their endocytosis was observed via confocal microscopy.

examined the impact of exosomes on the femoral head and found that they had positive effects.

Human umbilical cord MSCs (HUC-MSCs) are easily extracted from the umbilical cord and have stem cell-like properties, demonstrating remarkable potential for tissue regeneration. However, few researchers have studied the osteogenic effects of exosomes derived from HUC-MSCs in GIONFH. In this study, we examined the effects and mechanism of action of miR-365a-5p derived from exosomes produced by HUC-MSCs in the setting of GIONFH. A rat model was used to investigate the pathogenesis of GIONFH. In addition, the protective effects of HUC-MSC-derived exosomes were also investigated, mainly by transferring exosomal miR-365a-5p to inhibit SAV1 expression in the Hippo signaling pathway.

RESULTS

Characterization of HUC-MSC-Exos

To characterize the purified exosomes from HUC-MSCs, transmission electron microscopy (TEM), NanoSight analysis, and western blotting were used. TEM showed that HUC-MSC-Exos were round in shape with a size of approximately 100 nm and had a lipid bilayer membrane structure (Figure 1A). Western blotting showed that the surface markers of HUC-MSC-Exos, including CD9, CD63, CD81, and TSG101, were present (Figure 1B). NanoSight analysis revealed that the size distribution of these particles was approximately 100 nm (Figure 1C). In addition, the enrichment of exosomes was also examined, and the results showed that the exosomes were mainly enriched at 100 nm (Figure 1D). PKH26 was used to label exosomes, and the results of that experiment showed that PKH26-labeled HUC-MSC-Exos were found in BMSCs as a result of endocytosis (Figure 1D).

HUC-MSC-Exos promoted cell proliferation and osteogenesis

To study the effect of exosomes on cell proliferation, BMSCs were cultured in conditioned medium with or without 10 μM dexamethasone (Dex). The results of Cell Counting Kit-8 (CCK-8) assays showed that treatment decreased BMSC proliferation, and exosomes significantly increased the proliferation rate compared to Dex treatment (Figures 2A and 2B). To investigate the osteogenic effect of exosomes, we performed alizarin red staining and found that Dex can significantly inhibit calcium deposition. Exosomes can reverse the inhibitory effect of Dex (Figure 2C). In addition, western blotting was performed to investigate the expression of osteogenic markers, including BMP2, Runx2, and Sp7. These experiments revealed that the expression of osteoblast markers in the exosome intervention group was significantly higher than that in the Dex group (Figures 2D–2G). All of these data showed that HUC-MSC-Exos can reverse the inhibitory effect of Dex and promote cell proliferation and osteogenesis.

Exosomal miR-365a-5p was upregulated in HUC-MSC-Exos

As previously reported, miRNA is the most abundant component of exosomes.[9,10] To investigate the mechanism of the impact of HUC-

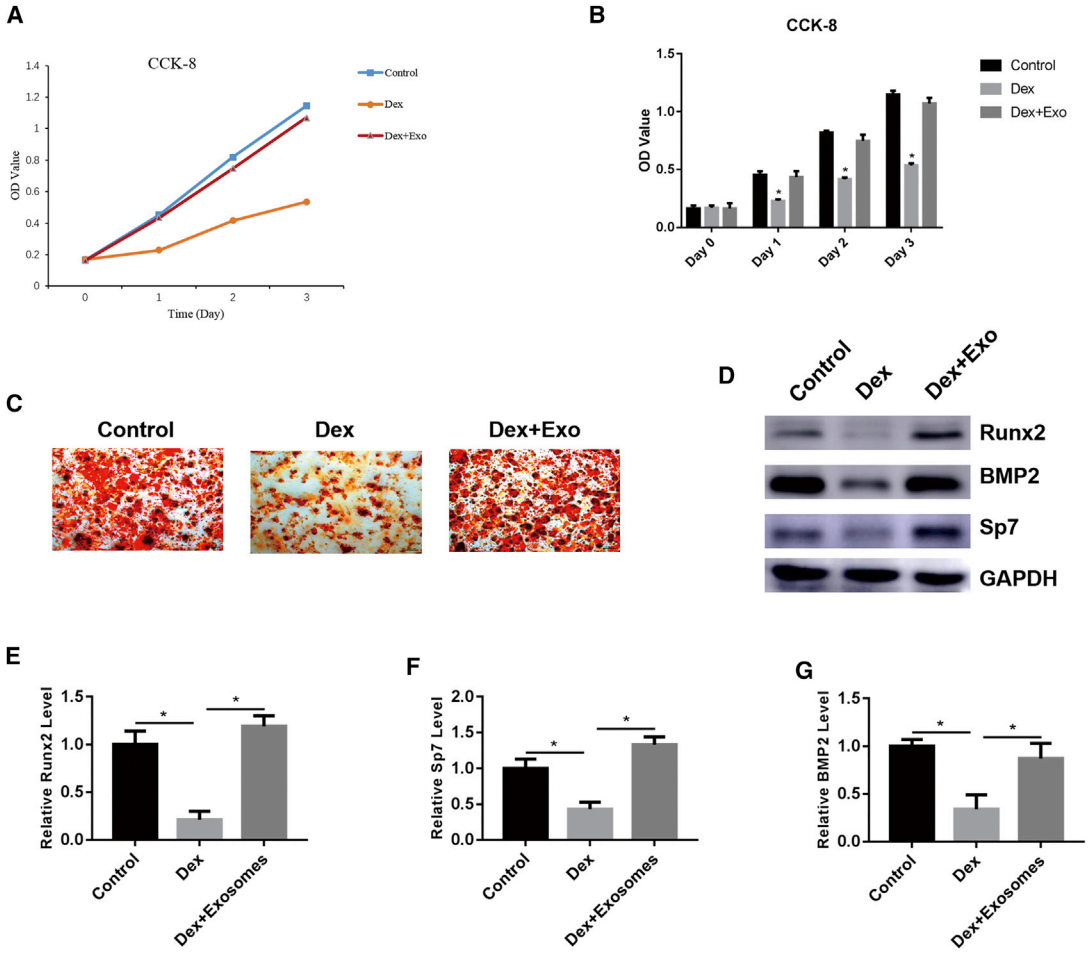

Figure 2. HUC-MSC-Exos promoted cell proliferation and osteogenesis as determined by CCK-8 assay, alizarin red staining, and western blotting

(A) BMSCs were cultured in conditioned medium containing Dex with or without exosomes, and proliferation was determined by a CCK-8 assay. (B) Statistical analysis was performed to investigate the proliferation rate. (C) Alizarin red staining was used to detect the osteogenesis of BMSCs treated with Dex with or without exosomes. Scale bars, 200 μm. (D) Western blotting was performed to detect the expression of Runx2, BMP2, and Sp7 in BMSCs treated with Dex with or without exosomes. (E–G) The relative levels of Runx2 (E), Sp7 (F), and BMP2 (G) were verified using ImageJ. *p < 0.05.The error bars stand for standard deviation. The scale bars stand for 220 μm.

MSC-Exos on cell proliferation and osteogenesis, we performed high-throughput miRNA sequencing to examine the differentially expressed miRNAs in the Dex (control group) and Dex+exosome group (experimental group). The results, displayed in a Venn diagram, revealed that 717 miRNAs were identical in the three control samples, and 697 miRNAs were identical in the three experimental samples (Figures 3A and 3B). The differentially expressed miRNAs in the control and experimental groups were also investigated, and the results revealed that 147 miRNAs were upregulated in the experimental group and 162 miRNAs were downregulated in the control group (Figure 3C). All of the significantly differentially expressed miRNAs are presented in a heatmap (Figure 3E), and miR-365a-5p expression was found to be significantly higher in the experimental group than in the control group, with a p value <0.0001. We also investigated signaling pathway enrichment, and the results showed that osteogenesis-related signaling pathways, including MAPK, mTOR, and HIF-1α, were enriched (Figure 3D). We also conducted a Gene Ontology analysis, the results of which revealed that exosomes mainly regulate gene networks related to signal transduction and endocrine and metabolic diseases (Figure 3F). Moreover, the candidate miRNAs were mainly located in the cytoplasm (Figures 3G and 3H). These data suggest that HUC-MSC-Exos may play an important role in osteogenesis via differentially expressed miRNAs.

miR-365a-5p was upregulated in HUC-MSC-Exos to bind SAV1

According to previous studies, exosomes contain a variety of genetic materials, including miRNAs, which play an important role in regulating cellular metabolism and proliferation. We screened published articles available online and found that miR-21,[11,12] miR-155,[13,14] miR-125b,[15,16] miR-122,[8] and miR-221-3p[17] produced by various stem cells were the exosomal miRNAs most frequently reported to regulate osteogenesis (Figure 4A). However, no studies have reported

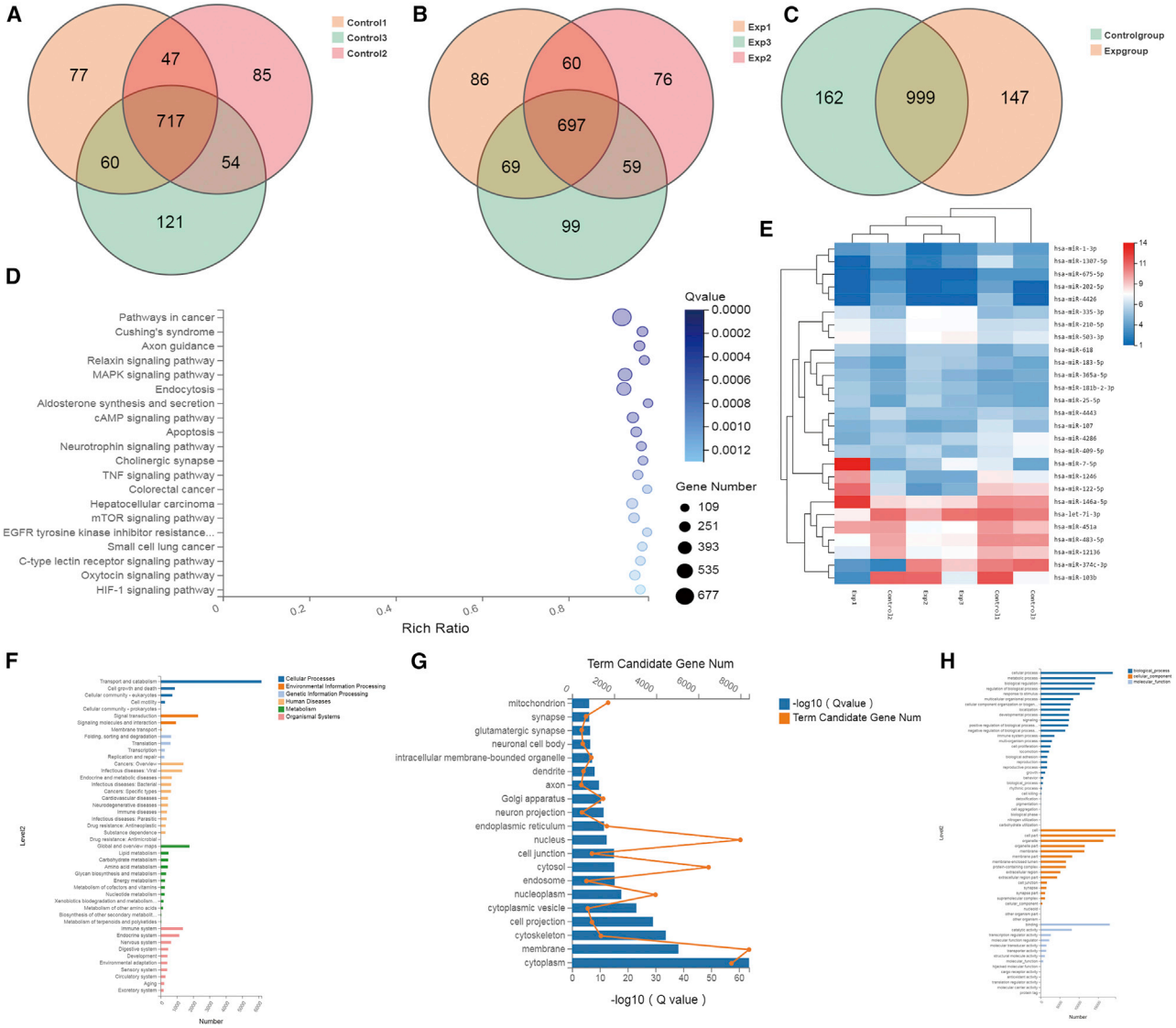

Figure 3. RNA-seq was performed to identify differentially expressed exosomal miRNAs

(A) miRNA expression in the control group is shown with a Venn diagram. (B) miRNA expression in the experimental group is shown with a Venn diagram. (C) Differential miRNA expression between the control and experimental groups is shown with a Venn diagram. (D) Kyoto Encyclopedia of Genes and Genomes (KEGG) pathway analysis was performed to evaluate the related signaling pathways. (E) Cluster analysis was performed in each group, and heatmaps were used to show the differential expression of miRNAs. (F) Differentially expressed genes were classified into biological pathways, and the metabolic pathways involved were divided into six groups as follows: cellular processes, environmental information processing, genetic information processing, human disease, metabolism, and organismal systems. (G) The candidate gene number term was calculated using the Q value. (H) Gene Ontology analysis was used for the functional classification of differentially expressed genes.

that exosomal miR-365a-5p derived from HUC-MSCs regulates osteogenesis. We first verified the enrichment of miR-365a-5p in exosomes, and qPCR results showed that the level of miR-365a-5p in HUC-MSC-Exos was 5.09-fold higher than that in Dex-treated exosomes (Figure 4B). Subsequently, we studied the changes in miR-365a-5p levels in BMSCs treated with HUC-MSC-Exos or PBS. The results revealed that the expression of miR-365a-5p was significantly upregulated in the HUC-MSC-Exos-treated group (Figure 4C). To explore the mechanism of action of miR-365a-5p, we examined its cellular localization using RNA fluorescence *in situ* hybridization (FISH) and found that it was mainly located in the cytoplasm (Figure 4J), a result consistent with the RNA sequencing (RNA-seq) results. Next, we investigated the downstream target of miR-365a-5p. The target of miR-365a-5p was predicted using a TargetScan database search, the results of which showed that miR-365a-5p interacts with SAV1 (Figure 4D). The transfection efficiency was evaluated by qPCR (Figures 4E and 4F). SAV1 is an important scaffold protein that regulates the Hippo signaling pathway.[18] When miR-365a-5p was

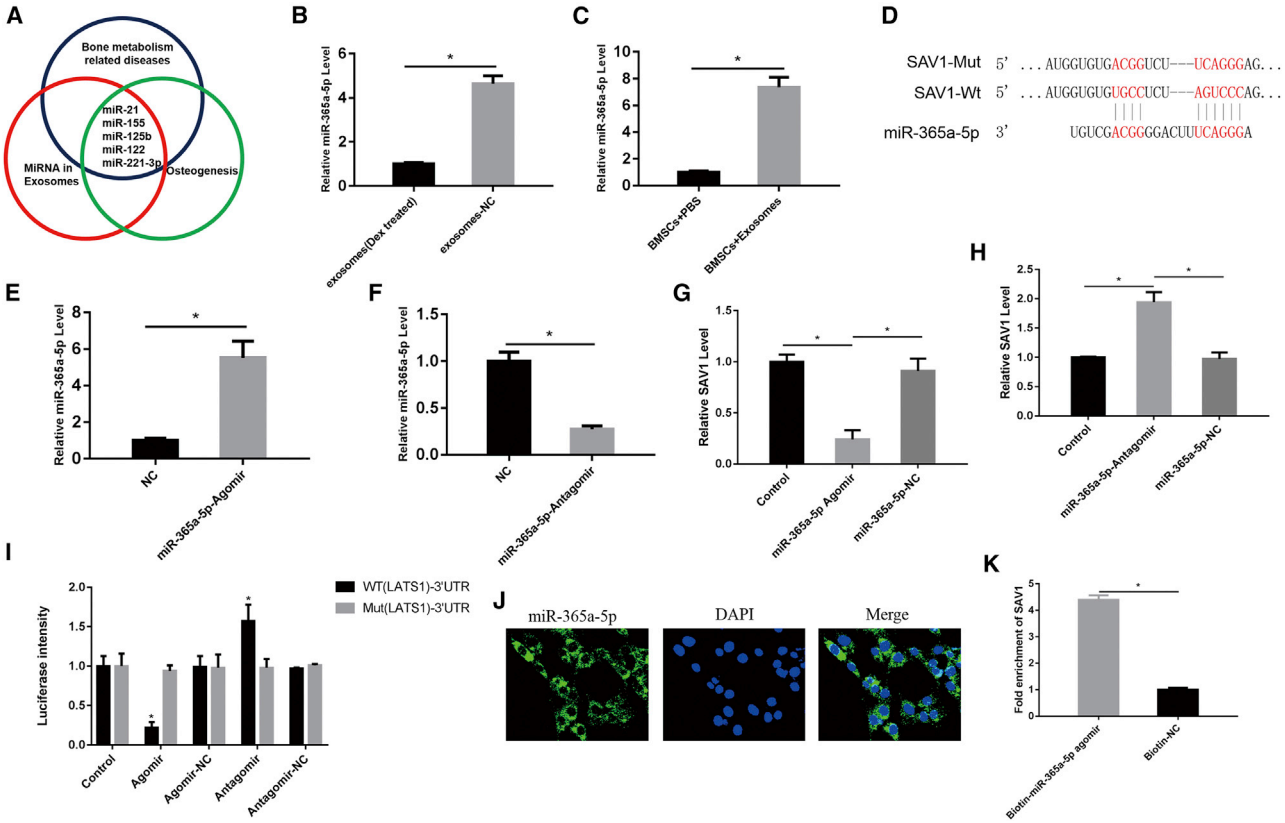

Figure 4. The interaction between miR-365a-5p and SAV1 was verified using qPCR, luciferase reporter assay, RNA pull-down, and RNA FISH

(A) The related miRNAs, such as miR-21, miR-155, miR-125b, miR-122 and miR-221-3p, participating in regulating bone metabolism and osteogenesis that are contained in exosomes. (B) RT-PCR was performed to detect the level of miR-365a-5p in Dex-treated exosomes and the negative control. (C) RT-PCR was performed to detect the level of miR-365a-5p in BMSCs cocultured with PBS or exosomes. (D) The miR-365a-5p-SAV1 binding site. (E and F) The transfection efficiency of the miR-365a-5p agomir (E) and miR-365a-5p antagomir (F) was evaluated using RT-PCR. (G) SAV1 expression was evaluated after transfection with miR-365a-5p agomir. (H) SAV1 expression was evaluated after transfection with miR-365a-5p antagomir. (I) A luciferase reporter assay was performed to verify the interaction between miR-365a-5p and SAV1. (J) RNA FISH was performed to detect the cellular location of miR-365a-5p. (K) The interaction between miR-365a-5p and SAV1 was investigated using RNA pull-down. *$p < 0.05$. The error bars stand for standard deviation.

upregulated, SAV1 expression was inhibited (Figure 4G). Downregulating miR-365a-5p increased the expression of SAV1 (Figure 4H). In addition, a dual-luciferase reporter assay also showed the interaction between miR-365a-5p and SAV1 (Figure 4I). An RNA pull-down assay was also performed, and the results showed that SAV1 can be pulled down using biotin-labeled miR-365a-5p (Figure 4K). All of these data showed that exosomal miR-365a-5p was upregulated in HUC-MSC-Exos and that it bound and inhibited SAV1.

We used GW4869 to inhibit the secretion of HUC-MSC-Exos, and qPCR was performed to detect the expression level of exosomal miR-365a-5p. The results showed that the amount of exosomal miR-365a-5p was decreased in the GW4869 group. Additionally, 5-ethynyl-2′-deoxyuridine (EdU) and alizarin red S (A-S) staining revealed that cellular proliferation and osteogenesis were decreased in the GW4869 group compared with the HUC-MSC-Exos group (Figure S1). We also transfected miR-365a-5p agomir into HUC-MSCs, extracted the exosomes, and detected significantly increased miR-365a-5p levels in the miR-365a-5p agomir group. Furthermore, EdU and A-S staining showed that cellular proliferation and osteogenesis were increased in the miR-365a-5p agomir group compared with the HUC-MSC-Exos group (Figure S2).

We screened the miRBase to obtain the precursor (pre-)miRNA sequence. We used NCBI BLAST to obtain the primary (pri-)miRNA sequence, and 100-bp upstream to downstream flanking sequences were acquired based on the pre-miRNA sequence. qPCR was performed to detect the levels of pri-miR-365a-5p and pre-miR-365a-5p. The results showed no significant differences between the BMSC and BMSC+Exos groups (Figure S3).

Exosomal miR-365a-5p regulated osteogenesis and proliferation through the Hippo signaling pathway

Western blotting was performed to detect downstream gene expression in the Hippo signaling pathway, and the results revealed that Dex can activate the expression of SAV1, LATS phosphorylation,

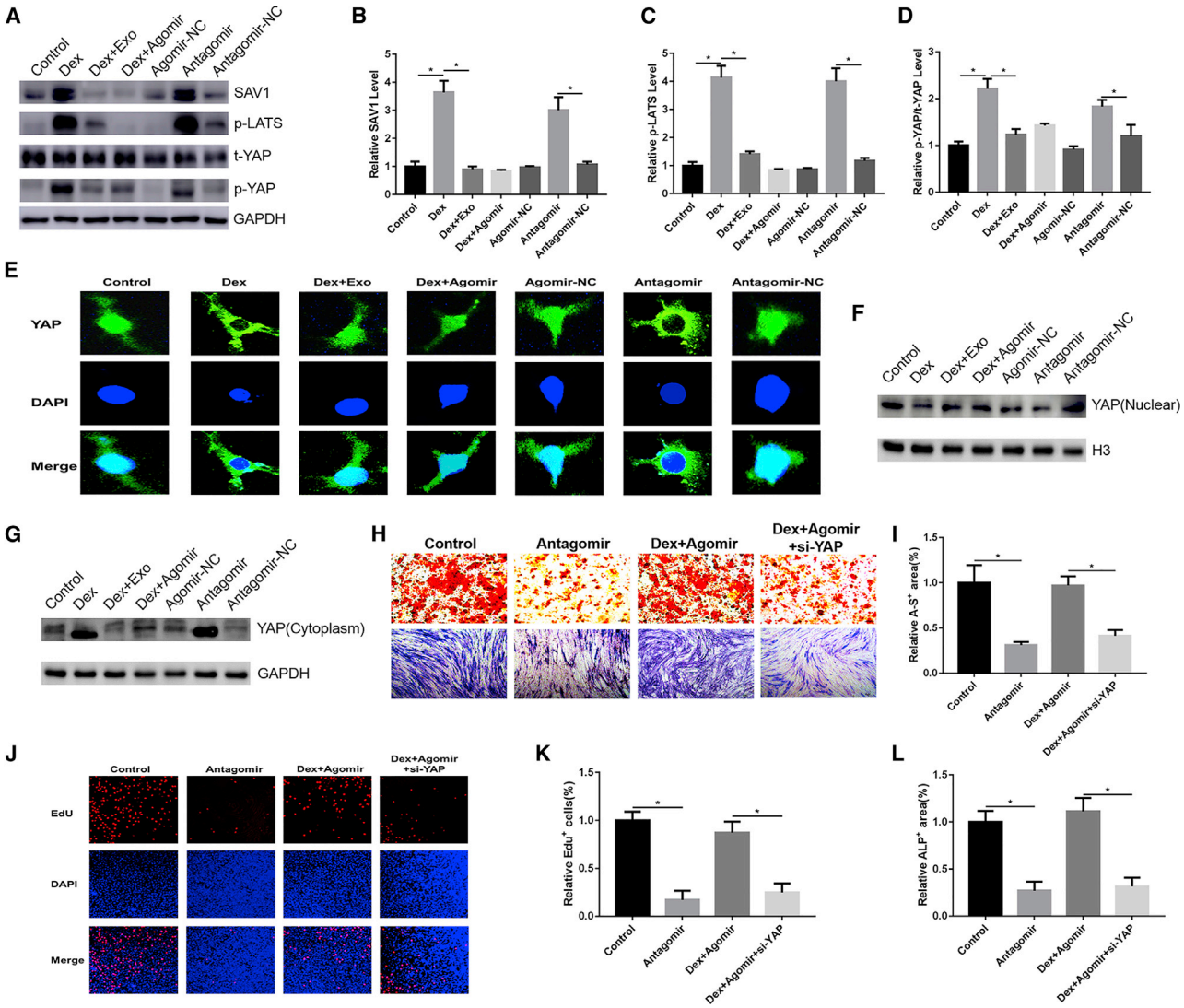

Figure 5. miR-365a-5p regulated osteogenesis through the Hippo signaling pathway

(A) Western blotting was used to detect the expression of related genes, including SAV1, p-LATS, total (t-)YAP, and p-YAP, in the Hippo signaling pathway. (B–D) ImageJ was used to calculate the expression of SAV1 (B), p-LATS (C), and p-YAP/t-YAP (D). (E) Immunofluorescence staining was performed to evaluate the nuclear and cytoplasmic location of YAP. (F) Western blotting was performed to evaluate the nuclear expression of YAP. (G) Western blotting was performed to evaluate the cytoplasmic expression of YAP. (H) Alizarin red staining and ALP staining were used to detect osteogenesis in BMSCs in the control, agomir, Dex+agomir, and Dex+antagomir+YAP small interfering RNA (si-YAP) groups. (I) Calculation of the alizarin red-positive area. (J) EdU staining was used to detect proliferation in the control, agomir, Dex+agomir, and Dex+-antagomir+si-YAP groups. (K) Calculation of the percentage of EdU-positive cells using ImageJ. (L) Calculation of the ALP-positive area. *$p < 0.05$. The error bars stand for standard deviation. The scale bars stand for 220μm.

and upregulate the expression of phosphorylated (p-)YAP. Exosomes reversed the effects of Dex treatment (Figures 5A–5D). The miR-365a-5p agomir also inhibited SAV1 expression, LATS phosphorylation, and YAP phosphorylation (Figures 5A–5D). When cells were transfected with the miR-365a-5p antagomir, the SAV1 expression was activated, LATS was phosphorylated, and p-YAP expression was upregulated (Figures 5A–5D). These results were verified by immunofluorescence staining (Figure 5E). Additionally, we explored the expression of YAP in the nucleus and cytoplasm. These results were consistent with immunofluorescence staining (Figures 5F and 5G). Next, we explored the osteogenic effect of miR-365a-5p using alkaline phosphatase (ALP) and alizarin red staining. The results showed that upregulation of miR-365a-5p can promote osteogenesis and downregulation of miR-365a-5p can inhibit osteogenesis. In addition, when YAP expression was inhibited, osteogenesis in the agomir+Dex group was inhibited (Figures 5H, 5I, and 5L). Proliferation was also investigated using EdU staining, and the results showed that downregulation of miR-365a-5p can inhibit the proliferation

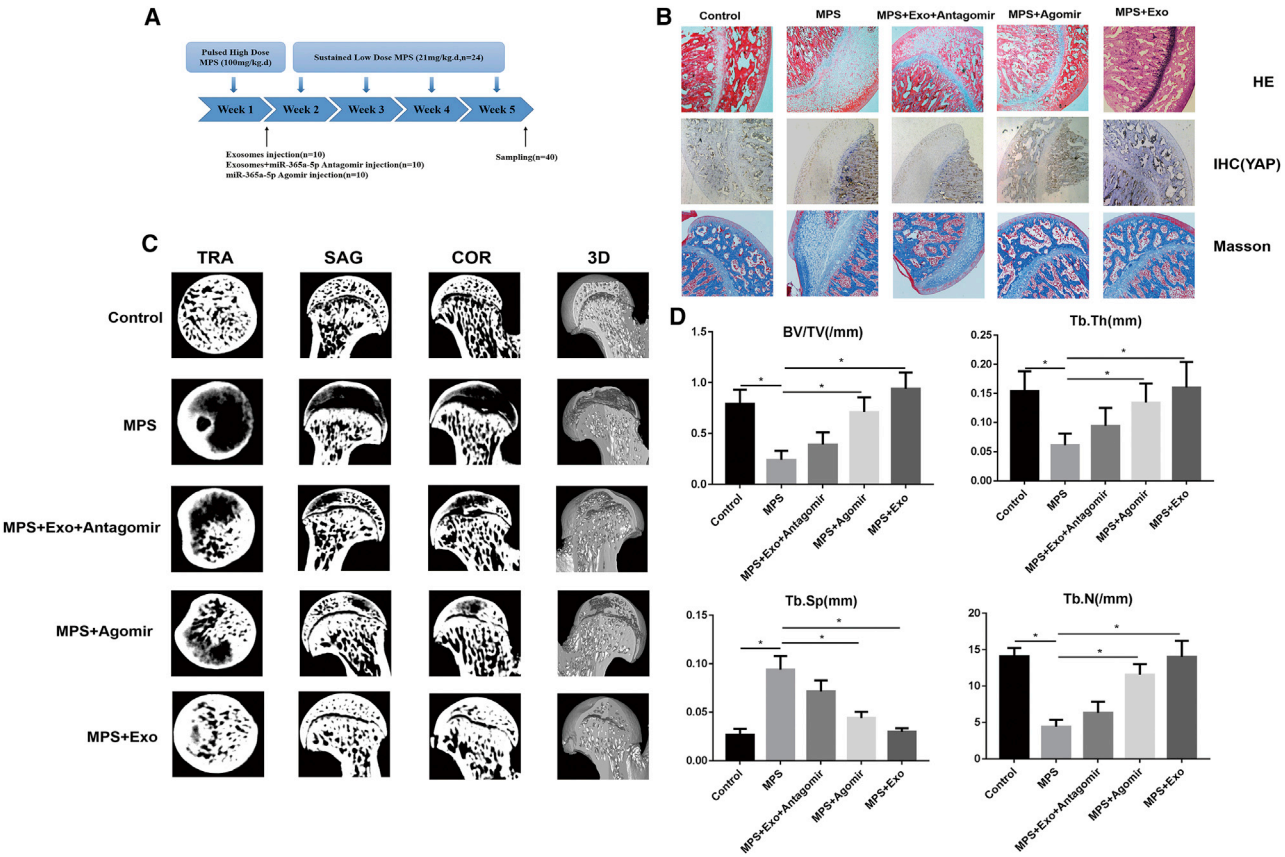

Figure 6. miR-365a-5p regulated osteogenesis in a GIONFH rat model

(A) Schematic of the MPS-induced GIONFH rat model and the different treatment groups. (B) H&E and Masson staining of the femoral heads of rats receiving different treatments. IHC staining was used to detect the level of YAP. (C) Micro-CT scans were performed to assess femoral head bone volume (BV) in the different treatment groups. (D) Quantitative analyses of BV per tissue volume (BV/TV), trabecular thickness (Tb.Th), trabecular separation (Tb.Sp), and trabecular number (Tb.N) in the different treatment groups. *$p < 0.05$. The error bars stand for standard deviation.

rate. When YAP expression was inhibited, proliferation in the agomir+Dex group was also inhibited (Figures 5J and 5K). All of these data suggested that exosomal miR-365a-5p regulated osteogenesis and proliferation through the Hippo signaling pathway. In addition, we explored the effect of SAV1 overexpression when cocultured with exosomes. The results of ALP and alizarin red staining showed that the osteogenic effect was inhibited when SAV1 was overexpressed (Figure S4).

HUC-MSC-Exos regulated GIONFH in a rat model through miR-365a-5p

To verify whether HUC-MSC-Exos can promote osteogenesis *in vivo*, we studied the effect of exosomes on the GIONFH model. The rat model of GIONFH was established using intramuscular methylprednisolone (MPS) injection, as presented in the schematic in Figure 6A. H&E and Masson staining demonstrated clear evidence of osteonecrosis in the MPS group, with sparse trabeculae in the femoral head and replacement with necrotic tissue. In contrast, the trabecular bones of rats in the MPS+exosome (MPS+Exo) and MPS+agomir groups were well organized, and few trabecular bones were replaced by necrotic tissue. In addition, when rats in the MPS+Exo group were transfected with miR-365a-5p antagomir, the area of osteonecrosis increased compared to the MPS+Exo group (Figure 6B). Immunohistochemistry (IHC) staining of YAP showed that femoral head YAP expression in the MPS and MPS+Exo+antagomir groups was significantly decreased, but this effect could also be reversed by the administration of exosomes and miR-365a-5p agomir (Figure 6B; Figure S5). Micro-computed tomography (micro-CT) was used to qualitatively evaluate the femoral head bone volume (BV) (Figure 6C). The results of micro-CT demonstrated that almost no trabecular bone was found in the MPS group, and the administration of exosomes and miR-365a-5p agomir significantly increased trabecular bone repair compared with the MPS group. The administration of miR-365a-5p antagomir significantly inhibited trabecular bone repair compared with the control group. In addition, the microstructure parameters BV/total volume (TV), trabecular thickness (Tb.Th), and trabecular number (Tb.N) in the MPS and MPS+Exo+antagomir groups were significantly lower than those in the exosome+MPS and control

groups. However, administration of miRNA agomir and exosomes could significantly reverse MPS-induced bone loss. In addition, compared with the control group, the trabecular separation (Tb.Sp) in the MPS group was significantly increased, and administration of miRNA agomir or exosomes could significantly decrease the Tb.Sp value. All of these data showed that HUC-MSC-Exos regulated GIONFH through miR-365a-5p in a rat model.

DISCUSSION

Bone is a dynamic tissue that is formed by osteoblasts and can be absorbed by osteoclasts throughout the life cycle. The dynamic balance of osteoblast and osteoclast metabolism is an important mechanism of bone structure adaptation and optimization of bone function.[19] The inhibition of osteoblasts and metabolic imbalance in bone tissue induced by GCs is one of the important mechanisms underlying steroid-induced ONFH. In our study, HUC-MSC-Exos mediated osteogenesis through the miR-365a-5p/SAV1/YAP axis and promoted bone regeneration and repair. Therefore, HUC-MSC-Exos play an important role in the induction of osteogenesis in GIONFH.

Several studies have reported the role played by GCs in the balance between osteogenesis and osteoclast formation in GIONFH.[20,21] However, BMSCs are the most important cells for bone regeneration. Xie et al.[22] found that one important reason for the development of ONFH is that GCs impair the function of osteoblasts and osteoclasts and weaken the osteogenic effect of osteoblasts. They damage the dynamic metabolic balance and upregulate the adipogenic potential of BMSCs. In our study, GCs significantly inhibited BMSC proliferation and their osteogenic function. We also studied the mechanism by which HUC-MSC-Exos promote the proliferation of BMSCs, and the miR-365a-5p/SAV1/YAP axis may be an important target pathway for the treatment of GIONFH.

The osteogenic effect of exosomes on bone regeneration and repair has also been demonstrated in previous studies. Zhang et al.[23] found that IPSC-MSC exosomes can promote the osteogenic differentiation of BMSCs by activating the phosphatidylinositol 3-kinase (PI3K)/Akt signaling pathway. Li et al.[24] found that exosomes from hASCs could promote the migration, proliferation, and osteogenic differentiation of BMSCs *in vitro*. The effect of exosomes on osteogenic differentiation *in vivo* was confirmed by the significant increase in the number of Runx2- and Ocn-positive cells. Liao et al.[8] showed that following overexpression of miR-122-5p, bone mineral density, trabecular volume, and mean Tb.Th of the femoral head increased, and that there was significant improvement in the necrotic femoral head. Therefore, exosomes overexpressing miR-122-5p may downregulate SPRY2 via the RTK/RAS/MAPK signaling pathway and attenuate the development of ONFH. We also screened databases to identify known exosomal miRNAs related to bone metabolism and osteogenesis. These known exosomal miRNAs, including miR-21, miR-155, miR-125b, miR-122, and miR-221-3p, derived from various kinds of stem cells, play an important role in osteogenesis and bone metabolism. The downstream target genes of these miRNAs include PTEN,[11] PDCD4,[25] KLF5,[26] and HIF-1α.[27] All of these genes were correlated with signaling pathways, such as the AKT signaling pathway, involved in cellular proliferation, cellular differentiation, or osteogenesis. However, no study has reported the effect and function of exosomal miRNA derived from HUC-MSCs. In our study, the results of RNA-seq showed that miR-365a-5p was a relatively unstudied miRNA in osteogenesis. Additionally, we verified its effect on the downstream gene SAV1, which is important in the Hippo signaling pathway. We have also demonstrated that HUC-MSC-Exos can inhibit the osteocyte apoptosis in GIONFH via targeting with miR-21-5p in our previous study.[28] In this study, we found that HUC-MSC-Exos can promote the proliferation and osteogenesis of BMSCs and reverse the effect induced by GCs. We confirmed the effect of HUC-MSC-Exos on the proliferation and osteogenesis of BMSCs by EdU staining, quantitative reverse-transcriptase PCR (qRT-PCR), ALP, and alizarin red staining.

We used bioinformatics analysis and RNA-seq technology to study the mechanism of action of exosomes' impacts on cell proliferation and osteogenesis. The RNA-seq results showed that miR-365a-5p was upregulated in HUC-MSC-Exos. To date, no studies have reported the effects of miR-365a-5p in GIONFH. We also found that the Hippo signaling pathway may be a key downstream regulator in GIONFH. YAP is an important transcription factor downstream of the Hippo signaling pathway. Many studies have reported that YAP is involved in cellular proliferation, differentiation, and tumorigenesis.[29–31] YAP plays a key role in inducing osteogenic differentiation and the differentiation of MSCs into osteoblasts by regulating the transcription factor Runx2.[32] Jiang et al.[33] found that the inhibition of miR-21-3p using human umbilical vein endothelial cell-derived exosomes could block Hippo signaling pathway-driven apoptosis in hypoxia/reoxygenation-treated neurons.

Furthermore, we explored the mechanism of YAP activation. Recent studies have shown that exosomes play a beneficial role in promoting cellular proliferation and cardiac fibroblasts (CF) phenotypic changes by inhibiting DUSP1 expression.[34] In our study, we found that the level of miR-365a-5p expression in extracellular vesicles secreted by HUC-MSCs was significantly higher than that in BMSC-derived exosomes, a finding that was validated by qPCR. In addition, we used a dual-luciferase reporter assay and RNA pull-down assay to confirm the interaction between miR-365a-5p and SAV1. SAV1 is a key regulator of LATS phosphorylation, and phosphorylated LATS can promote YAP/TAZ degradation to activate the Hippo signaling pathway.[35] We verified that exosomal miR-365a-5p regulates GIONFH through the Hippo signaling pathway. The effects of exosomal miR-365a-5p were verified using a rat model of GIONFH. Micro-CT as well as H&E, Masson, and IHC staining showed that exosomal miR-365a-5p could be used to promote the osteogenesis of GIONFH.

In conclusion, we explored the role of HUC-MSC-Exos in promoting the proliferation and osteogenesis of BMSCs. In addition, this study reported the mechanism underlying the impact of HUC-MSC-Exos

on the proliferation and osteogenesis of BMSCs through the miR-365a-5p/SAV1/YAP signaling pathway both *in vivo* and *in vitro*.

MATERIALS AND METHODS

Cell culture and treatment

HUC-MSCs were cultured and identified using flow cytometry as previously described.[11] BMSCs from the bone marrow of rats were extracted and cultured in α-minimum essential medium (α-MEM) supplemented with 10% fetal bovine serum (FBS) and 100 μg/mL penicillin/streptomycin.

BMSCs were treated with Dex, exosomes, or both to investigate the effects of exosomes derived from HUC-MSCs. The concentration of Dex used was 10 μM for 4 days for the CCK-8 analysis and 10 μM for 24 h for EdU staining. Ten μM Dex was administered for 21 days in the osteogenic differentiation assay. The concentration of exosomes was 50 μg/mL.

Exosome isolation, purification, and identification

First, we removed exosomes from FBS by overnight centrifugation at 110,000 × *g* and 4°C.[36,37] The medium without exosomes was prepared using α-DMEM and 10% exosome-free FBS. After adhering to the container wall, the supernatant was replaced with exosome-free medium. After 72 h of culture, we collected the supernatant from cultured HUC-MSCs. The residual cells were removed by centrifugation at 500 × *g* for 10 min. Then, the supernatant was filtered through a 0.22-μm filter. Finally, after ultracentrifugation at 120,000 × *g* for 70 min, the obtained precipitates were the exosomes. After resuspension in PBS, the exosomes were stored at −80°C.

Exosome diameter was analyzed by TEM (transmission electron microscope HT7700, Hitachi, Tokyo, Japan). The size distribution of exosomes was determined via NanoSizer technology (Malvern, UK). The specific exosome biomarkers CD9, CD63, CD81, and TSG101 were measured by western blotting.

PKH26-labeled exosomes

The exosomes were labeled with PKH26 (PKH26PCLMSDS, Sigma-Aldrich) according to the manufacturer's instructions. Briefly, under dark conditions, 250 μg of exosomes was fully re-suspended in 1 mL of C solution. In addition, the PKH26 solution was diluted into a 2×10^{-6} M working solution with 1 mL of C solution. After fully mixing the exosomes with the PKH26 working solution for 5 min, 2 mL of 5% BSA was added to the above mixture to neutralize the excess PKH26 dye. Finally, the exosome suspensions were labeled with PKH26 and centrifuged at 100,000 × *g* at 4°C for 70 min, and the final precipitate was suspended in 50 μL of PBS. A confocal microscope was used for imaging.

Cell viability assay

The CCK-8 assay (Beyotime Biotechnology) was performed to estimate the cell proliferation rate. A total of 3,000 BMSCs per well were seeded into 96-well plates. We detected the cell proliferation rate in different treatment groups, including the control, Dex, and Dex+exosomes groups. The optical density (OD) values were measured using an enzyme-linked immunosorbent assay reader (SpectraMax Plus 384, Molecular Devices, Sunnyvale, CA, USA) at 450 nm.

Alizarin red staining

Alizarin red staining was used to detect the osteogenic differentiation of BMSCs following different treatments. Osteogenic differentiation medium was used for osteogenesis as previously reported.[38] Briefly, the BMSCs were adjusted to a concentration of 10^4 cells/well and seeded into 12-well plates. The osteogenic culture medium supplemented with Dex or Dex+exosomes was changed every 48 h. We used 4% paraformaldehyde to fix the cells for 15 min after 21 days of induction. After washing three times using PBS, A-S dye was used for staining. After washing with distilled water three times, the cells were observed and imaged using a light microscope.

ALP staining

ALP staining was performed to evaluate the osteogenic effects as previously reported.[39] Osteogenic differentiation medium was used to induce osteogenesis. After 7 days of induction, the induced cells were fixed with 4% formaldehyde for 20 min. An ALP staining kit was used to measure ALP activity. After washing three times with PBS, ALP activity was measured by microscopy.

RNA FISH

RNA FISH was conducted as previously described.[11,40] The probe 5′-CACATCTGCCCCCAAAAGTCC-3′ was labeled with FAM and synthesized based on the sequence of miR-365a-5p. The *in situ* hybridization was then conducted per the FISH detection kit (QIAGEN) instructions. Images were acquired on a confocal fluorescence microscope.

miRNA transfection

miR-365a-5p agomir, antagomir, and negative control (Sangon Biotech, Shanghai, China) were transfected according to the manufacturer's guidelines. Here, 50 nM miR-365a-5p agomir and negative controls were used for the corresponding cell experiment. Additionally, 100 nM miRNA antagomir and negative controls were used for the corresponding cell experiment. Then, 10 μM miR-365a-5p agomir or antagomir was injected intramuscularly once a week in the GIONFH rat model.

Dual-luciferase reporter assay

Luciferase reporter analysis was carried out according to the protocol described previously.[13] The 5′-flanking sequence of the SAV1 promoter was inserted into a pGL3 vector. Then, the pGL3-SAV1 vector with 40 ng of pRL-TK vector was transfected into BMSCs using Lipofectamine 2000. The Dual-Luciferase reporter assay system was used to detect the luciferase intensity. Firefly luciferase activity was normalized to Renilla luciferase activity in each transfected well. In short, BMSCs were cotransfected with the indicated RNA oligonucleotides and reporter plasmids.

RNA pull-down assay

Biotin-miR-365a-5p mimics or blank controls were purchased from Sangon Biotech. When the cultured BMSCs reached 50%–60% confluence, biotin-miR-365a-5p mimics or controls were transfected into the BMSCs. After 48 h of transfection, the cells were harvested for pull-down assays. The biotin-coupled RNA complex was pulled down by incubating cell lysates with streptavidin-coated magnetic beads. qRT-PCR was used to evaluate the abundance of SAV1 in the bound fractions.

High-throughput miRNA sequencing

High-throughput RNA sequencing was performed to detect the expression of miRNA in the Dex-treated and Dex+exosome groups. Total RNA was extracted and purified using a miRNA extraction kit. Library construction and sequencing were carried out using BGISEQ-500 (BGI, Shenzhen, China). Differentially expressed miRNAs were calculated using a fold change cutoff of 2; the p value cutoff was <0.05. The bioinformatics services were provided by BGI.

Cell proliferation assay

Cellular proliferation was evaluated using EdU (RiboBio). Briefly, approximately 10^4 cells/well were seeded into glass plates and transfected for 24 h when the cell density reached 60%–70%. The EdU solution was diluted with cell culture medium at a ratio of 1,000:1, and each well was incubated with diluted EdU solution for approximately 3 h. After incubation with 50 μL of cell fixation solution (4% paraformaldehyde) at room temperature for 30 min, 50 μL of glycine was added to neutralize the EdU solution (at a concentration of 2 mg/mL). After washing with PBS three times, 100 μL of 1× Apollo staining solution was added to each well and cells were incubated away from light for 30 min. Then, 0.5% Triton X-100 was added and cells were incubated for 2 min. Finally, 100 μL of 1× Hoechst 3342 reaction solution was added to each well, and the cells were incubated at room temperature away from light for 30 min, then washed three times with 100 μL of PBS. The prepared cells were examined on a fluorescence microscope and imaged. Cell proliferation was evaluated by calculating the cell proliferation rate (cell proliferation rate % = number of EdU-positive cells/total number of cells).

Western blotting and antibodies

Protein samples were extracted from cells or bone tissue following essentially the same procedures described previously.[41] Briefly, protein from cells or bone tissue was cracked on ice with buckets of tissue/cell lysate (containing 1% PMSF) for 30 min. Then, the protein concentration was determined via the bicinchoninic acid (BCA) method, and the lysates were diluted at a ratio of 1:5 with 5× SDS buffer solution, boiled for 5 min at 95°C, and added whole to the gel. Samples were separated via SDS-polyacrylamide gel electrophoresis and transferred to a nitrocellulose membrane, then blocked with 5% skim milk for 3 h at room temperature. The polyvinylidene fluoride (PVDF) membrane was incubated with primary antibody at 4°C overnight and then washed with 1× Tris-buffered saline with Tween 20 (TBST) three times. Horseradish peroxidase (HRP)-labeled secondary antibody (1:5,000; Proteintech, SA00001-2) was added and the membrane was incubated at room temperature for 2 h after being washed with 1× TBST three times. Finally, a chemiluminescent detector was used for imaging.

Primary antibodies, including anti-CD9 (Abcam, ab92726), anti-Runx2 (Abcam, ab76959), anti-CD63 (Abcam, ab59479), anti-TSG101 (Abcam, 125011), anti-GAPDH (Proteintech, 10494-1-AP), anti-BMP2 (Abcam, ab14933), anti-Sp7 (Abcam, ab94744), anti-SAV1 (Abcam, ab172705), anti-p-LATS (Abcam, ab111344), anti-YAP (Abcam, ab52771), anti-p-YAP (Abcam, ab76252), and anti-CD81 (Proteintech, 14387-1-AP), were used for western blotting at a dilution of 1:1,000.

Real-time RT-PCR

Real-time RT-PCR was performed as previously described.[38] TRIzol (Invitrogen) was used to extract total RNA. cDNA synthesis was performed according to the reverse transcription kit (TaKaRa PrimeScript RT reagent kit) protocol, and real-time PCR was carried out using a Roche LightCycler 480 sequence detection system. GAPDH was used as the quantitative control mRNA. The $2^{-\Delta\Delta Ct}$ method was used to calculate the relative expression of each gene.[42]

Animal model

The animal experiments presented were authorized by the Animal Research Ethics Committee of Shandong Provincial Hospital and were conducted in accordance with the National Institutes of Health *Guidelines for the Care and Use of Laboratory Animals*. Fifty 8-week-old male Sprague-Dawley (SD) rats weighing 300 ± 20 g were used in this experiment. We randomly divided the rats into five groups: (1) control group (rats treated with PBS), (2) MPS group, (3) MPS+exosome group, (4) MPS+exosomes+-miR-365a-4p antagomir group, and (5) MPS+agomir group. To induce the GIONFH model in the rats, we intra-muscularly injected a pulsed high dose of 100 mg/kg/day MPS during the first week and then continued to inject MPS at a low dose (21 mg/kg/day).[43] Five weeks later, the rats were sacrificed, and the femoral head was evaluated via micro-CT and histomorphological analysis.

Micro-CT analysis

An Inveon micro-positron-emission tomography (PET)/CT instrument (Siemens, Berlin, Germany) was used for bone scanning as previously reported.[11] Briefly, we used the micro-CT to scan the femur from the femoral head to the femoral condyle. Three-dimensional structures of the femoral head were reconstructed, and calculations were carried out using Inveon analysis workstation software. BV/TV, Tb.Th, Tb.N, and Tb.Sp were used for bone quality determination.

Hematoxylin and eosin (H&E) staining

The femoral heads of the rats in each group were fixed with 4% paraformaldehyde, then decalcified using 10% EDTA. Subsequently, the samples were embedded in paraffin and sliced into 5-μm

sections. The samples were deparaffinized in xylene for 10 min and rehydrated via a graded series of ethanol treatments. Hematoxylin staining was performed for 5 min and samples were then rinsed with PBS three times. Eosin staining was performed for 1 min after treatment with 5% acetic acid for 1 min. A microscope was used for imaging.

IHC staining

We performed IHC staining to evaluate the expression of YAP in GIONFH and normal femoral bone tissue. Four percent formaldehyde was used to fix the femoral samples at room temperature for 7 days. The samples were then embedded in paraffin and sliced into 5-μm sections. The samples were deparaffinized in xylene for 10 min and rehydrated via a graded series of ethanol treatments. Subsequently, we used 3% hydrogen peroxide as a catalase quencher, and the tissue sections were blocked in 10% goat serum (Sigma-Aldrich) for 1 h. The sections were incubated at 4°C overnight with an anti-YAP antibody (1:200; Abcam, catalog no. ab52771). Next, we used a biotin-labeled secondary antibody (1:100; Proteintech, catalog no. SA00004-6) for staining, and the signal was amplified and visualized using the chromogen diaminobenzidine, followed by hematoxylin counterstaining.

Masson staining

Four percent formaldehyde was used to fix the femoral samples at room temperature for 7 days. The samples were then embedded in paraffin and sliced into 5-μm sections. The samples were deparaffinized in xylene for 10 min and rehydrated via a graded series of ethanol treatments. Weigert's iron hematoxylin staining was performed. Hydrochloric acid alcohol (1%) was used for differentiation for several seconds and rinsed with water for 2 min. The Ponceau red solution in the Masson staining kit was used to stain for 5 min, then the tissue sections were rinsed quickly with distilled water. After treatment with phosphomolybdic acid solution, the aniline blue solution was used for counterstaining for 5 min. A microscope was used for imaging.

Statistical analysis

All of these experiments were repeated at least three times. The data are shown as means ± standard deviation (SD). Means of two groups were compared by a Student's t test. Means of multiple groups were compared by one-way analysis of variance (Fisher's least significant difference [LSD] test). Statistical analysis was conducted using SPSS 20.0 (IBM, Armonk, NY, USA). p values <0.05 were considered statistically significant.

SUPPLEMENTAL INFORMATION

Supplemental Information can be found online at https://doi.org/10.1016/j.omtn.2020.12.006.

ACKNOWLEDGMENTS

This study was supported by grants from the Natural Science Foundation of Shandong Province (ZR2017MH120).

AUTHOR CONTRIBUTIONS

J.Q., A.B.W., and K.H.Z. conducted the experiments; D.C.W. and X.M.L. designed the experiments; M.J.K. and K.H.Z. wrote the paper; and D.L.S. and W.W.C. revised the draft and generated figures.

DECLARATION OF INTERESTS

The authors declare no competing interests.

REFERENCES

1. Kubo, T., Ueshima, K., Saito, M., Ishida, M., Arai, Y., and Fujiwara, H. (2016). Clinical and basic research on steroid-induced osteonecrosis of the femoral head in Japan. J. Orthop. Sci. *21*, 407–413.
2. Zhang, Q.Y., Li, Z.R., Gao, F.Q., and Sun, W. (2018). Pericollapse stage of osteonecrosis of the femoral head: a last chance for joint preservation. Chin. Med. J. (Engl.) *131*, 2589–2598.
3. Weinstein, R.S. (2012). Glucocorticoid-induced osteoporosis and osteonecrosis. Endocrinol. Metab. Clin. North Am. *41*, 595–611.
4. Burke, J., Kolhe, R., Hunter, M., Isales, C., Hamrick, M., and Fulzele, S. (2016). Stem cell-derived exosomes: a potential alternative therapeutic agent in orthopaedics. Stem Cells Int. *2016*, 5802529.
5. Tkach, M., and Théry, C. (2016). Communication by extracellular vesicles: where we are and where we need to go. Cell *164*, 1226–1232.
6. Zhang, Y., Hao, Z., Wang, P., Xia, Y., Wu, J., Xia, D., Fang, S., and Xu, S. (2019). Exosomes from human umbilical cord mesenchymal stem cells enhance fracture healing through HIF-1α-mediated promotion of angiogenesis in a rat model of stabilized fracture. Cell Prolif. *52*, e12570.
7. Tao, S.C., Yuan, T., Zhang, Y.L., Yin, W.J., Guo, S.C., and Zhang, C.Q. (2017). Exosomes derived from miR-140-5p-overexpressing human synovial mesenchymal stem cells enhance cartilage tissue regeneration and prevent osteoarthritis of the knee in a rat model. Theranostics *7*, 180–195.
8. Liao, W., Ning, Y., Xu, H.J., Zou, W.Z., Hu, J., Liu, X.Z., Yang, Y., and Li, Z.H. (2019). BMSC-derived exosomes carrying microRNA-122-5p promote proliferation of osteoblasts in osteonecrosis of the femoral head. Clin. Sci. (Lond.) *133*, 1955–1975.
9. Shao, H., Im, H., Castro, C.M., Breakefield, X., Weissleder, R., and Lee, H. (2018). New technologies for analysis of extracellular vesicles. Chem. Rev. *118*, 1917–1950.
10. Nawaz, M., Fatima, F., Vallabhaneni, K.C., Penfornis, P., Valadi, H., Ekström, K., Kholia, S., Whitt, J.D., Fernandes, J.D., Pochampally, R., et al. (2016). Extracellular vesicles: evolving factors in stem cell biology. Stem Cells Int. *2016*, 1073140.
11. Kuang, M.J., Huang, Y., Zhao, X.G., Zhang, R., Ma, J.X., Wang, D.C., and Ma, X.L. (2019). Exosomes derived from Wharton's jelly of human umbilical cord mesenchymal stem cells reduce osteocyte apoptosis in glucocorticoid-induced osteonecrosis of the femoral head in rats via the miR-21-PTEN-AKT signalling pathway. Int. J. Biol. Sci. *15*, 1861–1871.
12. Wei, F., Yang, S., Guo, Q., Zhang, X., Ren, D., Lv, T., and Xu, X. (2017). MicroRNA-21 regulates osteogenic differentiation of periodontal ligament stem cells by targeting Smad5. Sci. Rep. *7*, 16608.
13. Liu, H., Zhong, L., Yuan, T., Chen, S., Zhou, Y., An, L., Guo, Y., Fan, M., Li, Y., Sun, Y., et al. (2018). MicroRNA-155 inhibits the osteogenic differentiation of mesenchymal stem cells induced by BMP9 via downregulation of BMP signaling pathway. Int. J. Mol. Med. *41*, 3379–3393.
14. Wu, T., Xie, M., Wang, X., Jiang, X., Li, J., and Huang, H. (2012). miR-155 modulates TNF-α-inhibited osteogenic differentiation by targeting SOCS1 expression. Bone *51*, 498–505.
15. Huang, K., Fu, J., Zhou, W., Li, W., Dong, S., Yu, S., Hu, Z., Wang, H., and Xie, Z. (2014). MicroRNA-125b regulates osteogenic differentiation of mesenchymal stem cells by targeting Cbfβ in vitro. Biochimie *102*, 47–55.
16. Wang, H., Xie, Z., Hou, T., Li, Z., Huang, K., Gong, J., Zhou, W., Tang, K., Xu, J., and Dong, S. (2017). miR-125b regulates the osteogenic differentiation of human mesenchymal stem cells by targeting BMPR1b. Cell. Physiol. Biochem. *41*, 530–542.
17. Zhang, Y., Gao, Y., Cai, L., Li, F., Lou, Y., Xu, N., Kang, Y., and Yang, H. (2017). MicroRNA-221 is involved in the regulation of osteoporosis through regulates

RUNX2 protein expression and osteoblast differentiation. Am. J. Transl. Res. *9*, 126–135.

18. Hansen, C.G., Moroishi, T., and Guan, K.L. (2015). YAP and TAZ: a nexus for Hippo signaling and beyond. Trends Cell Biol. *25*, 499–513.
19. Dirckx, N., Moorer, M.C., Clemens, T.L., and Riddle, R.C. (2019). The role of osteoblasts in energy homeostasis. Nat. Rev. Endocrinol. *15*, 651–665.
20. Shi, C., Qi, J., Huang, P., Jiang, M., Zhou, Q., Zhou, H., Kang, H., Qian, N., Yang, Q., Guo, L., and Deng, L. (2014). MicroRNA-17/20a inhibits glucocorticoid-induced osteoclast differentiation and function through targeting RANKL expression in osteoblast cells. Bone *68*, 67–75.
21. Tokuyama, N., Hirose, J., Omata, Y., Yasui, T., Izawa, N., Matsumoto, T., Masuda, H., Ohmiya, T., Yasuda, H., Saito, T., et al. (2015). Individual and combining effects of anti-RANKL monoclonal antibody and teriparatide in ovariectomized mice. Bone Rep. *2*, 1–7.
22. Xie, X.H., Wang, X.L., Zhang, G., Liu, Z., Yao, D., Hung, L.K., Hung, V.W.Y., and Qin, L. (2011). Impaired bone healing in rabbits with steroid-induced osteonecrosis. J. Bone Joint Surg. Br. *93*, 558–565.
23. Zhang, J., Liu, X., Li, H., Chen, C., Hu, B., Niu, X., Li, Q., Zhao, B., Xie, Z., and Wang, Y. (2016). Exosomes/tricalcium phosphate combination scaffolds can enhance bone regeneration by activating the PI3K/Akt signaling pathway. Stem Cell Res. Ther. *7*, 136.
24. Li, W., Liu, Y., Zhang, P., Tang, Y., Zhou, M., Jiang, W., et al. (2018). Tissue-engineered bone immobilized with human adipose stem cells-derived exosomes promotes bone regeneration. ACS Appl. Mater. Interfaces *10*, 5240–5254.
25. Xiao, J., Pan, Y., Li, X.H., Yang, X.Y., Feng, Y.L., Tan, H.H., Jiang, L., Feng, J., and Yu, X.Y. (2016). Cardiac progenitor cell-derived exosomes prevent cardiomyocytes apoptosis through exosomal miR-21 by targeting PDCD4. Cell Death Dis. *7*, e2277.
26. Zheng, B., Yin, W.N., Suzuki, T., Zhang, X.H., Zhang, Y., Song, L.L., Jin, L.S., Zhan, H., Zhang, H., Li, J.S., and Wen, J.K. (2017). Exosome-mediated miR-155 transfer from smooth muscle cells to endothelial cells induces endothelial injury and promotes atherosclerosis. Mol. Ther. *25*, 1279–1294.
27. Li, H., Liu, D., Li, C., Zhou, S., Tian, D., Xiao, D., Zhang, H., Gao, F., and Huang, J. (2017). Exosomes secreted from mutant-HIF-1α-modified bone-marrow-derived mesenchymal stem cells attenuate early steroid-induced avascular necrosis of femoral head in rabbit. Cell Biol. Int. *41*, 1379–1390.
28. Yang, B.C., Kuang, M.J., Kang, J.Y., Zhao, J., Ma, J.X., and Ma, X.L. (2020). Human umbilical cord mesenchymal stem cell-derived exosomes act via the miR-1263/Mob1/Hippo signaling pathway to prevent apoptosis in disuse osteoporosis. Biochem. Biophys. Res. Commun. *524*, 883–889.
29. Jang, W., Kim, T., Koo, J.S., Kim, S.K., and Lim, D.S. (2017). Mechanical cue-induced YAP instructs Skp2-dependent cell cycle exit and oncogenic signaling. EMBO J. *36*, 2510–2528.
30. Pan, J.X., Xiong, L., Zhao, K., Zeng, P., Wang, B., Tang, F.L., Sun, D., Guo, H.H., Yang, X., Cui, S., et al. (2018). YAP promotes osteogenesis and suppresses adipogenic differentiation by regulating β-catenin signaling. Bone Res. *6*, 18.
31. Dethlefsen, C., Hansen, L.S., Lillelund, C., Andersen, C., Gehl, J., Christensen, J.F., Pedersen, B.K., and Hojman, P. (2017). Exercise-induced catecholamines activate the Hippo tumor suppressor pathway to reduce risks of breast cancer development. Cancer Res. *77*, 4894–4904.
32. Xiao, Z., and Quarles, L.D. (2015). Physiological mechanisms and therapeutic potential of bone mechanosensing. Rev. Endocr. Metab. Disord. *16*, 115–129.
33. Jiang, Y., Xie, H., Tu, W., Fang, H., Ji, C., Yan, T., Huang, H., Yu, C., Hu, Q., Gao, Z., and Lv, S. (2018). Exosomes secreted by HUVECs attenuate hypoxia/reoxygenation-induced apoptosis in neural cells by suppressing miR-21-3p. Am. J. Transl. Res. *10*, 3529–3541.
34. Shen, J., Xing, W., Liu, R., Zhang, Y., Xie, C., and Gong, F. (2019). miR-32-5p influences high glucose-induced cardiac fibroblast proliferation and phenotypic alteration by inhibiting DUSP1. BMC Mol. Biol. *20*, 21.
35. Johnson, R., and Halder, G. (2014). The two faces of Hippo: targeting the Hippo pathway for regenerative medicine and cancer treatment. Nat. Rev. Drug Discov. *13*, 63–79.
36. Han, C., Zhou, J., Liang, C., Liu, B., Pan, X., Zhang, Y., Wang, Y., Yan, B., Xie, W., Liu, F., et al. (2019). Human umbilical cord mesenchymal stem cell derived exosomes encapsulated in functional peptide hydrogels promote cardiac repair. Biomater. Sci. *7*, 2920–2933.
37. Peinado, H., Alečković, M., Lavotshkin, S., Matei, I., Costa-Silva, B., Moreno-Bueno, G., Hergueta-Redondo, M., Williams, C., García-Santos, G., Ghajar, C., et al. (2012). Melanoma exosomes educate bone marrow progenitor cells toward a pro-metastatic phenotype through MET. Nat. Med. *18*, 883–891.
38. Kuang, M.J., Zhang, W.H., He, W.W., Sun, L., Ma, J.X., Wang, D., and Ma, X.L. (2019). Naringin regulates bone metabolism in glucocorticoid-induced osteonecrosis of the femoral head via the Akt/Bad signal cascades. Chem. Biol. Interact. *304*, 97–105.
39. Rawadi, G., Vayssière, B., Dunn, F., Baron, R., and Roman-Roman, S. (2003). BMP-2 controls alkaline phosphatase expression and osteoblast mineralization by a Wnt autocrine loop. J. Bone Miner. Res. *18*, 1842–1853.
40. Kuang, M.J., Xing, F., Wang, D., Sun, L., Ma, J.X., and Ma, X.L. (2019). circUSP45 inhibited osteogenesis in glucocorticoid-induced osteonecrosis of femoral head by sponging miR-127-5p through PTEN/AKT signal pathway: experimental studies. Biochem. Biophys. Res. Commun. *509*, 255–261.
41. Tao, S.C., Yuan, T., Rui, B.Y., Zhu, Z.Z., Guo, S.C., and Zhang, C.Q. (2017). Exosomes derived from human platelet-rich plasma prevent apoptosis induced by glucocorticoid-associated endoplasmic reticulum stress in rat osteonecrosis of the femoral head via the Akt/Bad/Bcl-2 signal pathway. Theranostics *7*, 733–750.
42. Schmittgen, T.D., and Livak, K.J. (2008). Analyzing real-time PCR data by the comparative C_T method. Nat. Protoc. *3*, 1101–1108.
43. Zheng, L.Z., Wang, J.L., Kong, L., Huang, L., Tian, L., Pang, Q.Q., Wang, X.L., and Qin, L. (2018). Steroid-associated osteonecrosis animal model in rats. J. Orthop. Translat. *13*, 13–24.